Learning from Reality: Lessons from Centrifuge Models

M.D. Bolton
Department of Engineering, University of Cambridge

ABSTRACT: Time does not go round twice. Although we may expend great efforts in forensic engineering to determine the possible causes of disasters after they have occurred, we will never know the precise antecedents. But we should also ask ourselves how we can learn from failures in order that engineers in future may avoid similar problems. Centrifuge models can recreate geotechnical reality but at small scale, and in which the density and stress history of every piece of soil can be established. Models can be fully monitored as they fail. And model events are also practically repeatable except for controlled variations, so we can learn scientifically. Examples are given of slope and excavation failures. Lessons will be drawn which are relevant for the prevention of flowslides such as in Hong Kong at Sau Mau Ping, and the prevention of deep excavation failures such as occurred at Nicoll Highway in Singapore.

1 INTRODUCTION

When disasters have happened in the field the pressure to explain them, and to apportion blame, is often intense. Governments may set up some committee of inquiry within a legal framework. Otherwise the courts of criminal or civil law will pursue those who may be responsible. Academic experts are often invited as expert witnesses to reveal and review the facts of the case from a technical perspective. In adversarial legal systems different experts may be appointed by each of the parties involved, such as the procurer of the scheme, the authority who sanctioned it, the designer, the construction companies, and those who have been injured or suffered loss.

However, because the original job would have been regarded as rather routine, and the disaster not foreseen, the information available later regarding the site investigation and construction procedure will usually contain omissions that prevent accurate back-analysis. Even the design to which the contractors were working may be contentious. Discovery of the original ground conditions will be hindered by the failure that has intervened. Highly significant geotechnical parameters, such as the pore water pressures in the ground that moved, may have changed from those which led up to the disaster. These inevitable difficulties will make any explanation of the disaster hypothetical. Each party may be able to propose a different hypothesis advantageous to their defense.

The main objective of the lawyers must be to establish liability, with the assistance of expert witnesses. Engineers should accept a deeper responsibility: to consider the underlying contributory factors, to clarify all the key mechanisms, and to propose improvements in education, training and professional practice so that the probability of a recurrence is minimized.

This paper will advocate the use of centrifuge models to achieve the goal of clarifying and simplifying behavior mechanisms, so as to improve future decision-making. Some may think it is strange that a disaster in the field should lead to research work in the laboratory. However, centrifuge researchers see model-scale “failures” every time they do a test. Most forensic geotechnics actually takes place in centrifuge laboratories.

2 RAINFALL-INDUCED FLOWSLIDES

Ten years ago, the author collaborated with the Hong Kong Government Geotechnical Engineering Office (GEO) in an attempt to throw more light on the mechanisms involved in fast flowslide failures which had been a problem in Hong Kong for many years. Loose fill slopes, which could be both steep and high, would occasionally fail dramatically after a period of intense rainfall. An example is the landslide at Sau Mau Ping on 25 August 1976 and shown in Figure 1. The foundation of the GEO in 1977 arose directly from the recommendations of the Review Panel. And a precept of the GEOs US$2B program of Landslip Preventive Measures, was the notion that these most dangerous flowslides were caused by static soil liquefaction triggered by a wetting front (Knill et al 1977).

Figure 1 Sau Mau Ping slope failure: view behind Block 9 (Binnie and Partners, 1976)

Centrifuge tests were conducted by an engineer on leave from GEO (Yeung, 2002), focusing on steep homogeneous slopes of loose completely decomposed granite (CDG) fill subjected to model rainfall. Neither liquefaction nor flowslides were observed. Instead, there was compaction due to wetting. On reflection, it was realized that the relatively low probability of a flowslide event, notwithstanding the relatively high frequency of intense rainstorms affecting loose fill slopes in Hong Kong, must indicate that some extra condition was required for their initiation.

A second GEO engineer (Wong, 2003) constructed tests on stratified CDG slopes, in which a buried coarse layer could be filled by water supplied directly at its crest, whilst being sealed by a layer of finer material. Figure 2 shows such a centrifuge model which was instrumented with miniature pore pressure transducers, and observed through a window on the cross-section. Digital cameras enabled PIV (White et al, 2003) to display the initiation of slipping, as shown in Figure 3, but the webcam which was used to record the subsequent fast flowslides was insufficient for the analysis of these much faster events.

Nevertheless, many useful insights were gained (Take et al, 2004). A simplified triggering mechanism was deduced, as shown in Figure 4. Water entering the coarse layer at high elevation percolates quickly to its base where it is prevented from escaping by the finer overburden. As the piezometric level rises (A→B→C) the internal effective stresses fall and slope movements increase. Eventually, the trapped water pressure mobilizes the sliding blocks. Hydro-fractures can also occur, as shown in Figure 4, but trapped water finds it difficult to escape since the landslide debris will always tend to cover it.

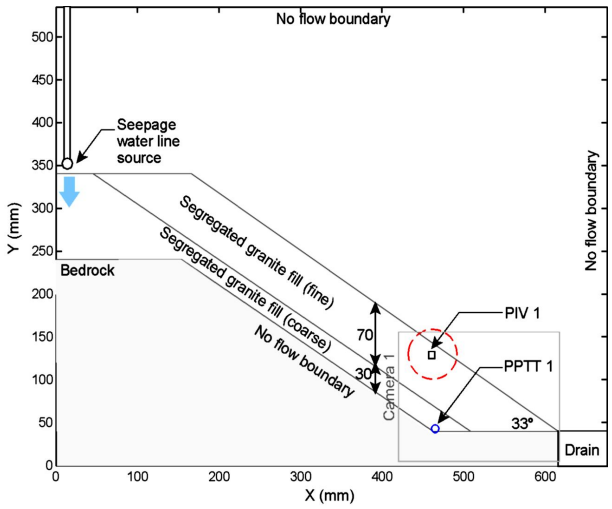

Figure 2 Model of fill slope with interior drainage layer (Wong, 2003)

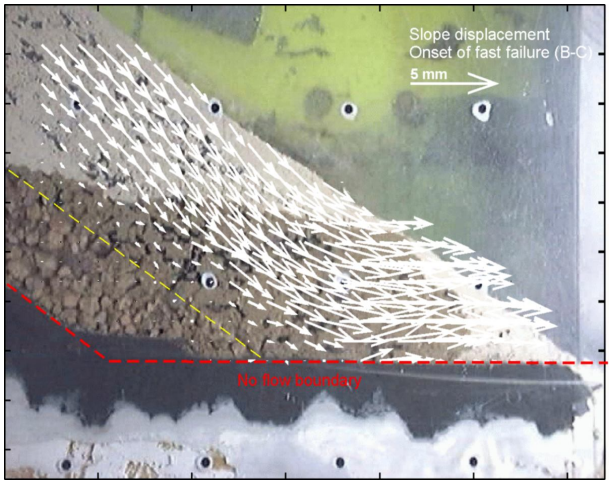

Figure 3 Trapped water initiates slope failure in loose fill, viewed using PIV (Take et al, 2004)

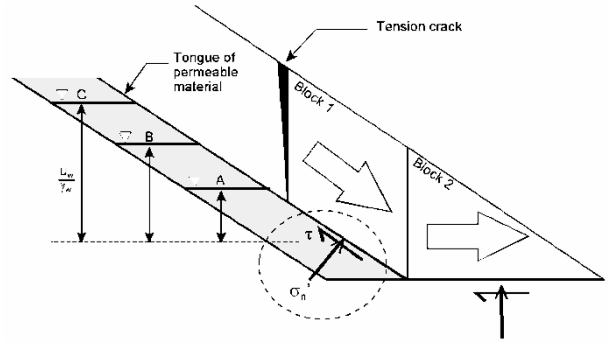

Figure 4 Simplified failure mechanism due to trapped water (Take et al, 2004)

The slope begins to fail due to water pressures building up inside the toe, but these water pressures are not immediately relieved by the failure, so the movement continues. Any dense zones of soil dilate and soften, so the mass strength of the moving soil reduces. The initial slip therefore accelerates, and its influence retrogresses so that the whole slope becomes mobile, and the slip becomes a flowslide or avalanche. Wong's tests with a granular reservoir inside the toe of a steep slope ended in a flowslide, whether the CDG fill covering it was loose or dense.

Figure 5 shows a frame taken just before the strong acceleration of the slippage induced by stored water below dense CDG fill. The stored water makes the granular layer darker in the picture than the dense, fine CDG overburden. It can also be seen in Figure 5 that a preferential flow path through the dense fill forms in the tension crack region suggested in Figure 4, such that the detached toe of the slope must be forced forward by the additional hydraulic thrust. After the flowslide had taken place, it could be seen that half of the fine CDG covering the slope had travelled down at high speed and departed to the right. The remaining material is shown in Figure 6, where a "pipe" can be seen to have formed below the debris, ultimately allowing water to escape. This again demonstrates that high pressure water was available to lubricate the base of the flowslide while it was taking place (Take et al, 2004).

A later centrifuge model study (Lee, 2005) also investigated layering of CDG and the ponding of "storm water" under the slope, but with the cut-off to the permeable reservoir located higher, at a mid-slope elevation. A similar *slip* mechanism was triggered, but in this case the ponded water quickly escaped onto the slope surface. The result was a mid-slope blow-out with some local slipping above it, but without any *flowslide* (Lee et al, 2008). This appears to confirm that flowslides in steep terrain will be most likely to occur when intense rain falling on a mountain can percolate downwards and be stored temporarily in a permeable layer beneath a less permeable soil slope, such that the foot of the permeable layer lies at or beneath the toe of the slope, and where the rate of percolation into the permeable layer during a storm can exceed the rate of leakage from it.

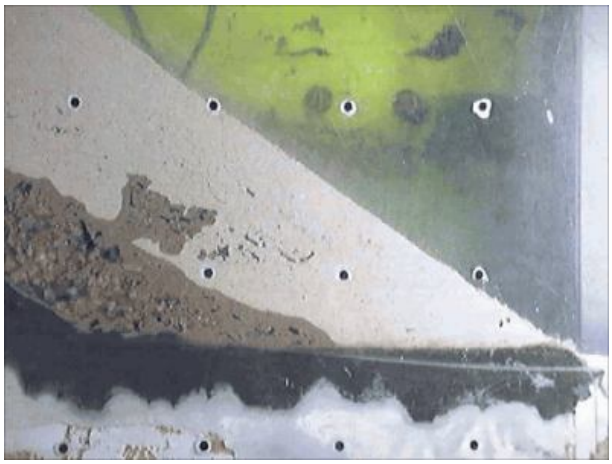

Figure 5 Development of internal hydro-fractures following slip initiation by trapped water in dense CDG (Wong, 2003)

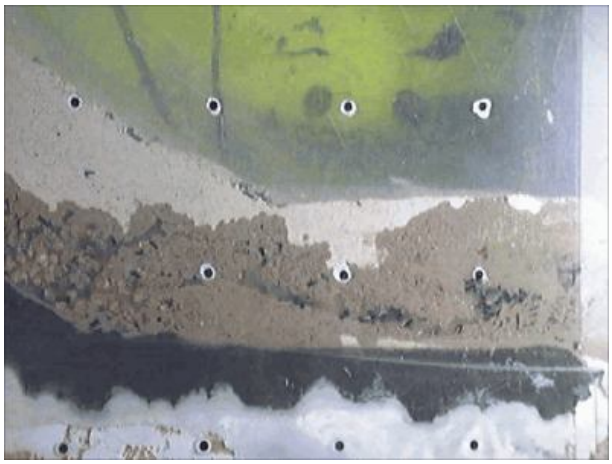

Figure 6 Trace of stored water escaping beneath fast flowslide in dense CDG (Wong, 2003)

This is an application where the observation of a complex deformation mechanism in a series of centrifuge tests needs the additional introduction of a simplified mechanism in order to clarify its potential role in decision-making. A complex finite element analysis of buried channels could have been carried out, of course, but this might have detracted from the explanatory power of the observed mechanism. The centrifuge model with trapped water seems to be an excellent representation of the catastrophic rainfall-induced landslide at Sau Mau Ping, with granular material

avalanching down a slope and then travelling fast along a horizontal plane. Furthermore, the presumably rare conjunction of buried permeable layers which are supplied by storm water from above and cut off at the elevation of the toe of the slope, seems to offer the right balance between improbability and possibility to explain the occasional observation of storm-induced flowslides of this sort.

Nevertheless, the GEO apparently felt unable to accept that an adequate countermeasure to flowsliding might lie in the insertion of horizontal drains at the toes of slopes, so as to tap into any trapped aquifers that might exist there. GEO preferred to adhere to the original supposition of static liquefaction caused by wetting, even though a variety of attempts to create it had been unsuccessful. They therefore continued in the LPM program to temporarily remove all zones of loose steep fill, place a drainage blanket on the slope, and compact the fill back in place, without performing any site-specific calculations. Although very expensive, this "one size fits all" policy has eliminated landslides where it has been applied. The topic of this paper is the possibility of observing real events in centrifuge models and then deducing simplified mechanisms which can be used for flexible and economic decision-making.

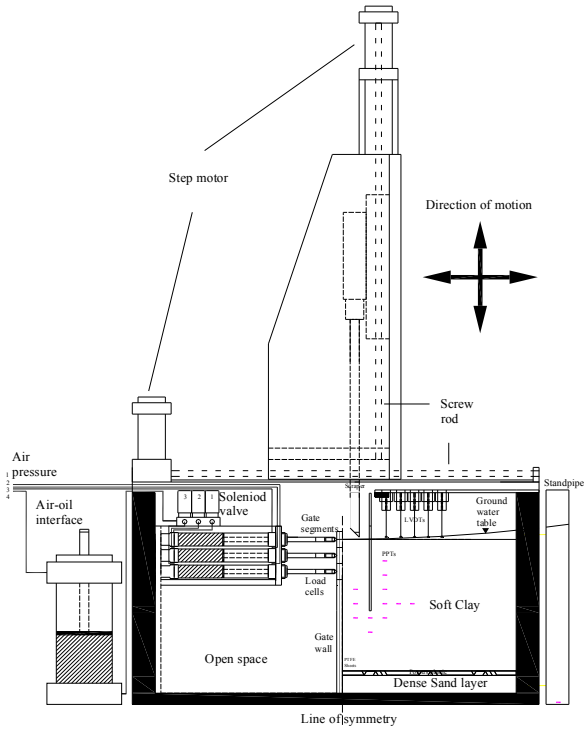

Figure 7 Centrifuge model package for excavations cut and propped in flight (Lam et al, 2011)

3 LIMITING GROUND MOVEMENTS

3.1 *Ground movements due to deep excavation*

Haigh et al (2010) describes the development of a twin axis servo actuator to work at up to 100g in a geotechnical centrifuge. Figure 7 illustrates its use in a plane strain centrifuge package, to excavate clay. A narrow blade can be lowered (in the analogue vertical sense) a few millimeters into a clay bed, and then translated sideways, so as to scrape clay into a preselected disposal area. Continuing incrementally, a model cliff face in clay, originally forming the boundary of a disposal area, can be advanced into a new location as clay spoil is scraped progressively into the disposal site.

Lam et al (2011) describe the use of this 2D actuator for research on the ground movements associated with braced excavations in clay. In this case, the original location of the scraper should be just in front of an instrumented model retaining wall. The disposal area falls behind an articulated low-friction gate-wall representing the centerline of a deep excavation. This gate-wall is successively demolished as the scraper removes both clay and wall segments, in stages, depositing both into the disposal area.

The articulated gate-wall is initially supported by a system of hydraulic struts acting in pairs at pre-set levels. These pairs of struts can be retracted in sequence, allowing the scraper both to remove a layer of clay and to knock down a gate segment as it is moved laterally away from the retaining wall. Once the top of the scraper blade has dropped below the level of a pair of props, they can be redeployed above it so as to support the retaining wall. The end result is a retaining wall supported at various levels by props which have been placed as the process of excavation continued with the centrifuge in flight. This allowed a more realistic construction sequence to be followed compared with the centrifuge modeling of excavation by draining a heavy fluid, such as described by Bolton and Powrie (1987).

Lam (2010) details a number of such centrifuge tests carried out at 60g on lightly overconsolidated kaolin clay which had initially been allowed to come into equilibrium with a high water table. Models were viewed on a cross-section through a Perspex window, with black sand grains creating texture on the white clay behind the window, as described earlier. Two digital cameras recorded ground movements, which were analyzed stage by stage using PIV. Models were also instrumented with displacement transducers, pore pressure

transducers, bending moment gauges on the retaining wall, and load cells mounted on the props. The focus here will be on the deformations which were observed at various stages of excavation, for walls of differing bending stiffness. Figure 8 shows three examples of patterns of wall and soil movements. In Figure 8(a) the model is portraying the initial response to excavation against a model diaphragm wall, prior to the deployment of any props. Essentially, the wall acts as a cantilever rotating about its toe; it also flexes outwards slightly at the top. The soil deformations on the active side of the wall resemble those described in much earlier centrifuge tests by Bolton and Powrie (1988). Those on the passive side are blocked somewhat by the narrower zone of excavation which leads to a squeezing and upwards extrusion, rather than to a triangular zone of shearing.

Figure 8(b) shows the outcome of excavating below a single high-level prop. The prop is not perfectly stiff, so the wall does move outwards a little at that location. However, the major mechanism is one of wall rotation about the prop, with evidence of the passive resistance at the foot of the wall causing it to deflect backwards relative to a simple rotation. The displacement vectors high on the active side are correspondingly steeper than in the unpropped case, but with the tendency to rotate at depth. There is an even more pronounced squeezing and upwards extrusion of clay on the passive side.

Figure 8(c) illustrates the response to excavation beneath multiple props. Since the wall acts as a continuous beam over multiple supports, it tends simply to bulge below the lowest prop. And considering the length of wall projecting below the lowest prop, the lower part of the wall behaves as though it is fixed at its base. This tendency is even more marked when the wall is toed in to a stiffer base stratum.

These patterns of deformation are broadly consistent with those found from field monitoring.

3.2 *Mobilizable Strength Design (MSD)*

The simplification and generalization of these mechanisms has been attempted in a series of papers that apply an approach called the Mobilizable Strength Design (MSD) method: Osman and Bolton (2006), Bolton et al (2008), Bolton et al (2010) and Lam and Bolton (2011).

The objective of MSD is to create a repertoire of mechanisms that can be used at any strain magnitude, and which must therefore avoid slip surfaces. Examples of finite-strain deformation mechanisms are given in Figure 9.

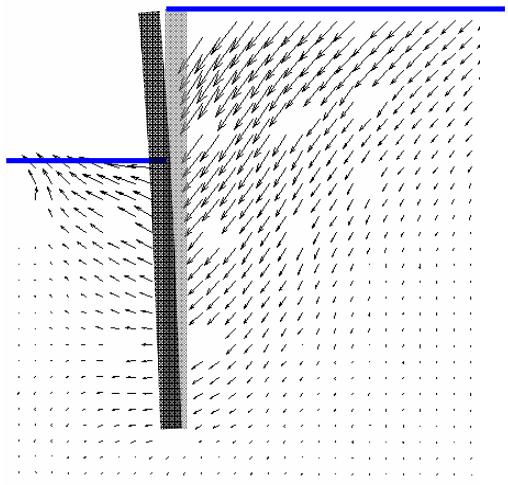

(a) Excavation against a cantilever wall

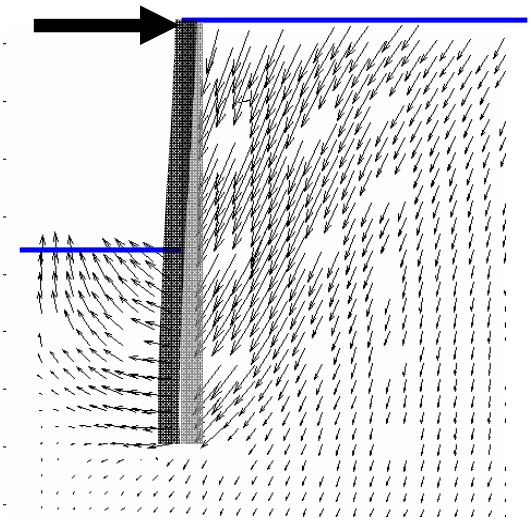

(b) Excavation against a propped cantilever wall

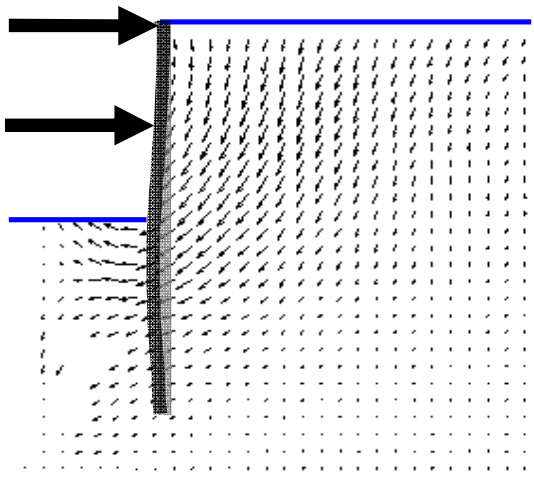

(c) Excavation against a multi-propped wall

Figure 8 Observed patterns of incremental wall deformation depending on wall stiffness and propping conditions during excavation (Lam et al, 2011)

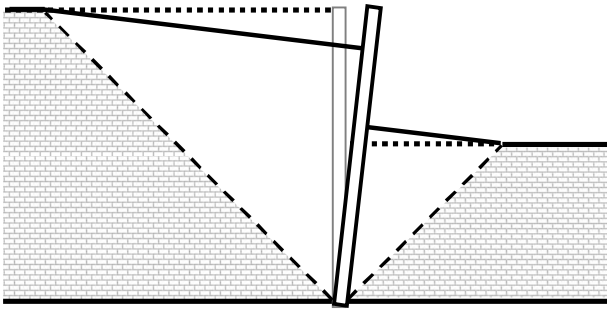

(a) Constant-strain triangles compatible with rigid wall rotation about the toe

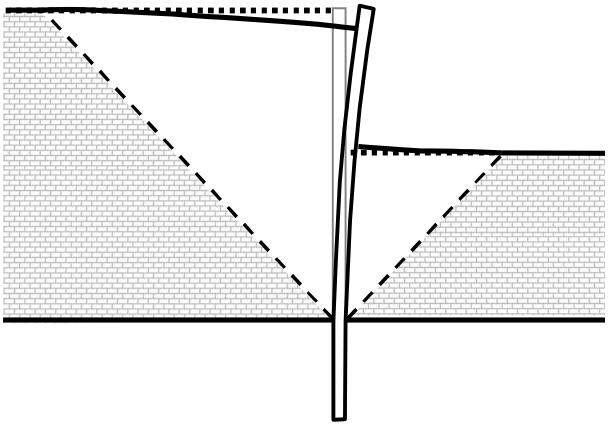

(b) Variable-strain triangles compatible with flexure of a wall that is fixed in a hard base layer

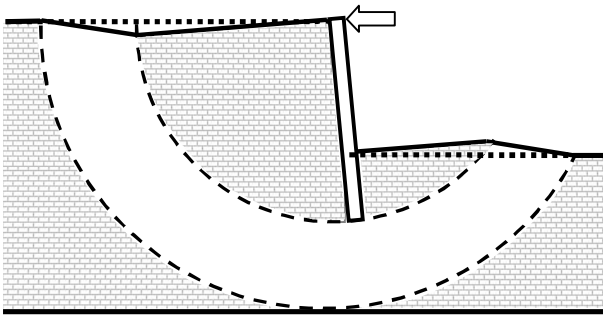

(c) Concentric shearing compatible with rotation about the top prop of a rigid "floating" wall

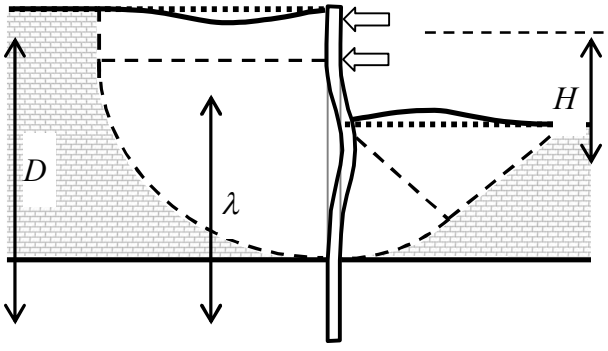

(d) Sinusoidal plastic flow compatible with a propped wall bulging into a wide excavation

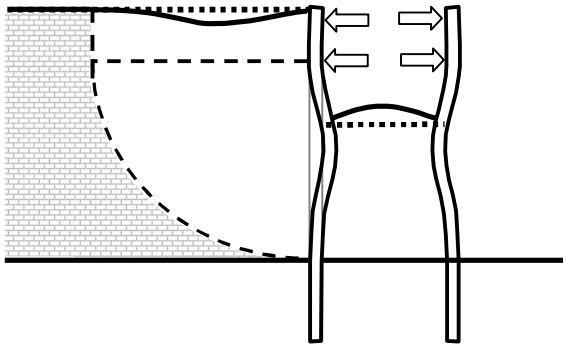

(e) Sinusoidal plastic flow compatible with a propped wall bulging into a narrow excavation

Figure 9 Simplified deformation mechanisms for various propping conditions during excavation

In each case there is a zone within which the deformation field is to be specified, while deformations in the shaded zones are ignored for simplicity.

These mechanisms require that the soil deforms at constant volume – "undrained" in the context of clays deforming during excavation. They can be used to produce approximate solutions for ground deformations in a fashion analogous to the use of slip circles in collapse limit analysis. And just as with limiting equilibrium solutions, therefore, these "limiting deformation" solutions need to be checked against FEA, centrifuge models, or field records to ensure that they are adequate.

The first application of MSD was to rigid, smooth, cantilever retaining walls in clay: Bolton and Powrie (1988). The wall was supposed to respond to excavation by rotating about a point just above its toe, creating active and passive zones either side, but restricting the strength to a value $c_{mob} < c_u$. The equations of lateral and moment equilibrium were written down and solved for c_{mob}. The mobilised shear strain γ could then be read off a representative stress-strain curve, and the wall rotation θ could be deduced from the relation $\gamma = 2\theta$, derived from Mohr's circle of strain. Centrifuge model tests showed that this approach provided reasonable accuracy, notwithstanding the simplifications of focusing only on near-field soil deformations, similar to Figure 9(a), and ignoring the influence of wall roughness.

A follow-up study by Osman and Bolton (2004) compared MSD based on wall rotation with FEA for "floating" cantilever walls, and showed that the influence of $K_o \neq 1$ could be accounted for if the data of compression and extension tests were separately available. Neither wall friction nor the precise shape of a soil's stress strain curve caused MSD calculations to depart excessively from FEA

computations. However, one factor not included in the MSD wall rotation model was significant in the FEA: the base of the wall translated towards the excavation. Effectively, FEA showed that a "floating" wall analysis invoking only wall rotation as in Figure 9(a) caused MSD to underestimate wall crest displacements by up to a factor of 2. MSD needs to include wall bending as in Figure 9(b), and deep foundation shearing as in Figure 9(c), if more precise predictions are to be made.

These aspects were considered by Osman and Bolton (2005) and Lam and Bolton (2011) in the application of MSD to braced excavations, specifically addressing the bulging that is seen below the bottom row of props when the excavation is advanced. Each increment of bulging can be predicted reasonably well by assuming the bulge to be sinusoidal, following O'Rourke (1993). Figures 9(d) for wide excavations and 9(e) for narrow excavations show a wall fixed in a hard layer, for which the wavelength of the bulge at any stage of excavation equals the distance between the bottom row of props and the bottom of the soft clay. Where there is no hard layer, virtual fixity can be imagined at a depth below the wall base equal to half the unsupported wall length below the bottom prop. Wall displacement calculations begin with the cantilever stage as shown in Figure 9(a) while an excavation is made for the top level of props. Progressive displacements are found by superposing each stage of wall bulging as in Figure 9(d) while excavation proceeds below the most recently fixed row of struts. Calculated wall displacements fell within ± 30% of field records.

These predictions of flexural deformation required a different calculation method based on the conservation of energy within the deformation mechanism, as first set out by Bolton et al (2008). The loss of potential energy, represented by the formation of a subsidence trough in the retained ground while the soil within the excavation heaves, must be balanced by the work done deforming both the soil and the retaining structure.

The loss of potential energy during any given stage of excavation is quite easily calculated as:

$$\Delta P = \Sigma\, (\rho g\, \Delta z)\, \delta A \qquad (1)$$

where the weight $\rho g\, \delta A$ of each element of soil of area δA within the mechanism is associated with its average settlement Δz. Each settlement Δz must be deduced from the sinusoidal displacement profile "flowing" through the mechanism in that stage.

The work done on the soil is calculated using the swept area under the soil's stress-strain curve. For example, the work done per unit area in straining soil by amount γ along a parabola with its apex at the origin, and passing through (c_u, γ_u) is:

$$\delta W_{soil} = \frac{2}{3}\tau\,\gamma = \frac{2}{3} c_u \left(\frac{\gamma}{\gamma_u}\right)^{0.5} \gamma = \frac{2}{3}\frac{c_u}{\gamma_u^{0.5}}\gamma^{1.5} \qquad (2)$$

The magnitude of strain γ has to be calculated from the sinusoidal displacement field. Then the total work done on the soil, starting from an undeformed state, is found by integration over the whole area of the mechanism:

$$\Delta W_{soil} = \Sigma\, \delta W_{soil}\, \delta A \qquad (3)$$

The work done in bending the wall from its initially undeformed state is calculated from the area under the moment-curvature relation. For a wall segment of unit length with a flexural stiffness EI developing a curvature κ:

$$\delta W_{wall} = \frac{1}{2} M\, \kappa = \frac{1}{2} EI\, \kappa^2 \qquad (4)$$

The magnitude of curvature is calculated from the second differential of the sinusoidal wall deflections. Then the total flexural work is found by integrating over the length of the wall:

$$\Delta W_{wall} = \int \delta W_{wall}\, dx \qquad (5)$$

The fundamental energy conservation equation of MSD is then, simply:

$$\Delta P = \Delta W_{soil} + \Delta W_{wall} \qquad (6)$$

This can be solved iteratively for each stage of excavation, using the maximum wall displacement Δw_{max} in that stage as the unknown. The subsidence increment is the same. Finally, these increments can be superposed to obtain the overall maximum displacement w_{max}.

Bolton et al (2008) took care to recognise the incremental and non-linear nature of this energy balance in the calculations they advanced. It is necessary to store the previous shear strain of each element of soil so that the work done due to the next increment of excavation can properly be calculated with respect to the non-linear stress-strain curve. A similar sort of procedure has to be used for the structural strain energy since this is also non-linear, having a quadratic relation to wall displacement and curvature.

Other important details were addressed, including the need to use a different mechanism when the excavation is narrow compared with its depth, and the use of a stratified ground model. In this fashion, they could compare MSD predictions of braced excavations with those of FEA conducted by Jen (1998) for a "floating" wall, with

the parameters recorded in Figure 10. Typical bulging wall profiles from Bolton et al (2008) are compared in Figure 11 for a 17.5 m deep excavation supported at 2.5 m intervals, against a 40 m deep wall in a 100 m deep profile modelled as Boston Blue Clay. Excavation width B varied from 30 m to 60 m.

Although MSD, working in a matter of minutes on a spreadsheet, does not precisely accord with Jen's FEA, the correspondence is close enough for decision-making purposes. The two pre-requisites for success are to have a compendium of simplified deformation mechanisms for compatible soil-structure interaction which are sufficiently close to reality, and to be able to characterise the ground in relation to its density, strength profile and stress-strain relation. If these aspects are well-represented the MSD analysis can hardly go wrong, because the principle of conservation of energy can hardly be faulted.

3.3 *Validating MSD analyses using site data*

A new database of 155 case histories has been compiled: Lam and Bolton (2011). Studies from nine cities are included: Bangkok (2 sites), Boston (5), Chicago (10), Mexico City (1), Oslo (9), San Francisco (4), Shanghai (67), Singapore (21) and Taipei (36). Full details and references will be found in Lam (2010).

These cases focused on the deformation of braced walls supporting deep excavations in soft to firm clays (i.e. $c_u < 75$kPa). In each case, information was extracted on soil properties, groundwater conditions, excavation geometry, structural support stiffness, and construction method. A total of 110 case histories were so fully documented that an analysis could be made with MSD allowing for stratification, the undrained strength profile of the clay, its stress-strain behaviour, and the elevation of assumed fixity in the base stratum.

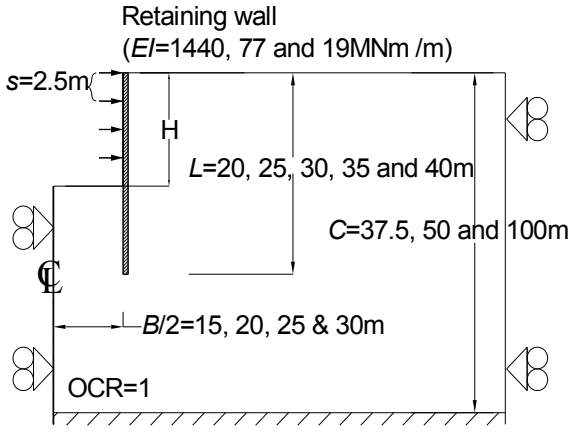

Figure 10 FEA carried out by Jen (1998)

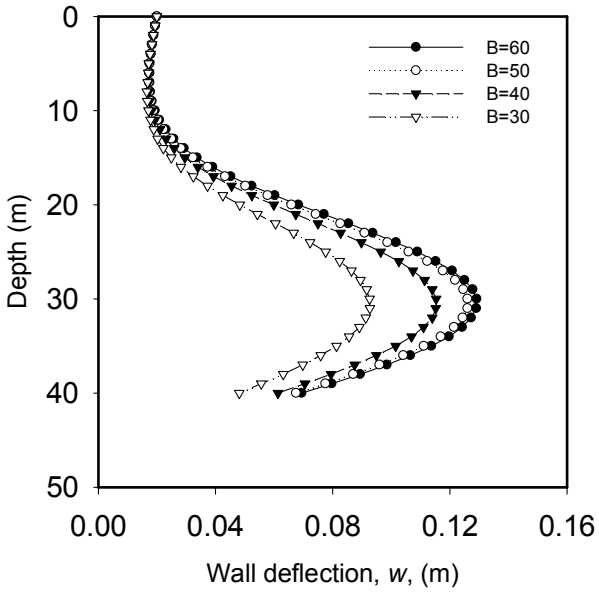

(a) Prediction by MSD (after Lam, 2010)

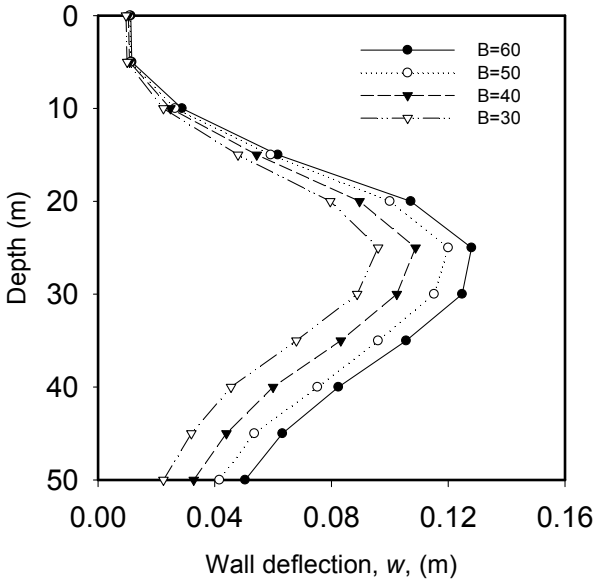

(b) Prediction by MIT E3 model (after Jen,1998)

Figure 11 Wall deflections for various widths B

Figure 12 shows the mobilization of shear strength versus strain as reported for the nine soils concerned. Parabolic shear stress-strain curves with strains to failure γ_u in the range 1% to 5% evidently provide a useful (if approximate) fit to the data at moderate strains. The information from the database was used directly in MSD to predict maximum wall displacements w_{max} for each stage of excavation, which are compared with authors' reported observations in Figure 13. Results show a correlation coefficient $R^2 = 0.91$ about the line 1:1. More than 90% of the MSD predictions fell within a factor of 1.4 of the corresponding observations. The field performance of MSD may be considered satisfactory: Lam and Bolton (2011).

3.4 *Using MSD to derive dimensionless groups*

Whilst MSD can confidently be used to make site-specific predictions, it will also be helpful to use MSD concepts to derive dimensionless groups to chart data from field case studies, and to assist decision-making prior to any detailed analysis. Consider first the normalization of maximum wall displacement w_{max} itself. MSD shows us, as in Figure 11, that the initial excavation to fix the top row of props generally produces relatively small movements at the crest in the cantilever phase of wall rotation or bending as sketched in Figures 9(a) and (b). The most significant deformations for a fixed-base wall arise from later stages of construction when the wall bulges below the lowest props, as sketched in Figures 9(d) and (e). Elastic beam theory applied to the mechanism then teaches us that the change of net pressure necessary to produce a bulge of amplitude w_{max} over a wavelength λ will be (Bolton et al, 2010):

$$\Delta p \propto w_{\max} \frac{EI}{\lambda^4} \tag{7}$$

This can be normalised with respect to the reduction in vertical earth pressure ρgH due to excavation. Accordingly, a structural response ratio S can be defined:

$$S = \frac{w_{\max} EI}{\rho g H \lambda^4} \tag{8}$$

Whilst MSD permits λ to reduce progressively as props are placed deeper, a design chart might simply characterise the average situation. An average λ value will be taken here as the distance between the middle props and the base of the deforming clay. Referring to Figure 9(d), we will use the following definition of average λ in equation 8.:

$$\lambda_{average} = D - 0.5H \tag{9}$$

Now consider the various system parameters that might modify the structural response ratio. It is proposed that they can best be visualised in combination as a soil-structure stiffness ratio R:

$$R = \frac{c_u}{\gamma_u} \frac{c_u}{\rho g H} \frac{\lambda^3}{EI} \tag{10}$$

Where an average λ is taken from (9), and where the value of c_u is selected to represent the strength at mid-depth of the soft clay layer.

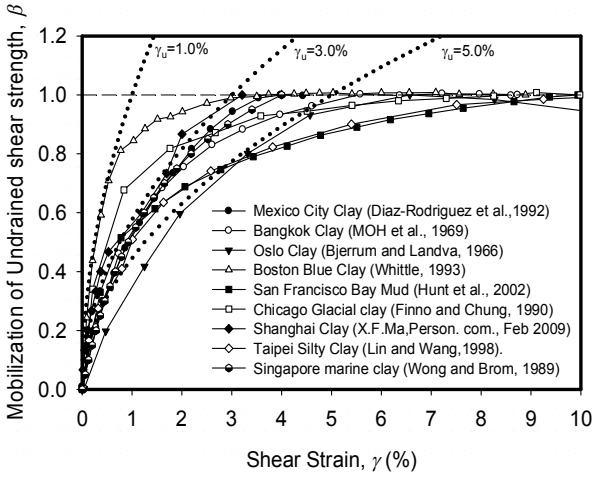

Figure 12 Stress-strain plots compared with parabolas

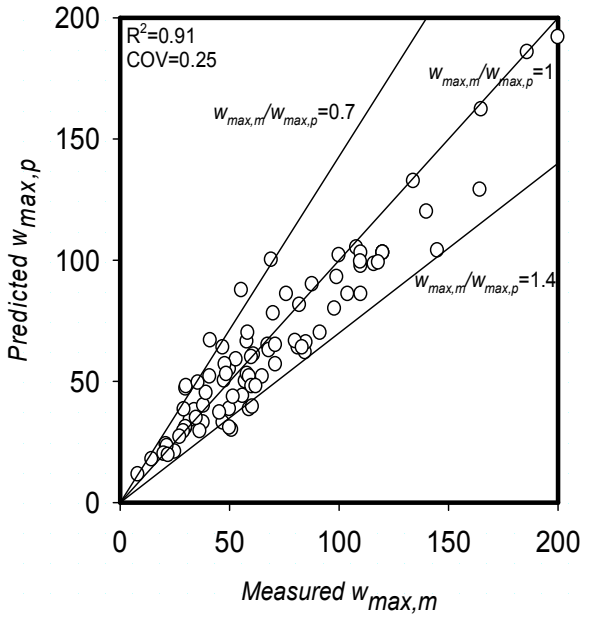

Figure 13 Performance of MSD predictions of w_{max}

The rationalisation is as follows. The ratio c_u/γ_u is the secant shear modulus just as peak strength is reached. For a parabolic shear stress-strain curve we obtain the secant modulus mobilised at any earlier stage:

$$G = \frac{c_{mob}}{\gamma} = \frac{c_u}{\gamma}\left(\frac{\gamma}{\gamma_u}\right)^{0.5} = \frac{c_u}{\gamma_u}\left(\frac{\gamma_u}{\gamma}\right)^{0.5} \tag{11}$$

We can write this as:

$$G = \frac{c_u}{\gamma_u}\frac{c_u}{c_{mob}} = \frac{c_u}{\gamma_u} M \tag{12}$$

representing the shear modulus increasing at higher values of M and correspondingly smaller strains.

Now, the average mobilisation factor M in the soil should be of the following form:

$$M \propto \frac{c_u}{\rho g H} \tag{13}$$

governing the "factor of safety" of an undrained excavation. It follows from (12) and (13) that the mobilised soil secant modulus:

$$G \propto \frac{c_u}{\gamma_u}\frac{c_u}{\rho g H} \tag{14}$$

which is recognisable as the first two terms on the right hand side of equation 10. The final term (λ^3/EI) is simply the inverse of wall bending stiffness per unit length, expressed in consistent units. Equation 10 therefore represents the non-dimensional soil-structure stiffness ratio for soil with a parabolic stress-strain curve up to (c_u, γ_u).

The new database can now be used to investigate the relationship between structural response ratio S and soil-structure stiffness ratio R: see Figure 14 where this is shown on log-log axes to capture the enormous range of wall stiffness between sheet-piles and diaphragm walls. Remarkably, the field data fit an exactly inverse relationship (i.e. the slope equals -1.00), with a coefficient of determination $R^2 = 0.964$:

$$\log_{10} S = -2.6 - \log_{10} R \tag{15}$$

This can be rationalised to give:

$$SR \approx \frac{1}{400} \tag{16}$$

within an uncertainty factor of 2.9 (calculated as 2 standard deviations) according to Figure 14. The same relationship emerges from the predicted wall displacements using MSD: see Figure 15.

Substituting for S and R from equations 8 and 10 respectively, we can define a normalised displacement factor ψ such that:

$$\psi = SR = \frac{w_{\max}}{\lambda}\frac{1}{\gamma_u}\left(\frac{c_u}{\rho g H}\right)^2 \approx \frac{1}{400} \tag{17}$$

Notably, the wall bending stiffness has now cancelled. Figures 14 and 15 have shown that wall stiffness has a negligible influence on the amplitude of wall bulging due to excavation. This has been proved for EI ranging within 4 orders of magnitude between sheet-piles and reinforced concrete diaphragms, representing 110 braced retaining walls from around the world.

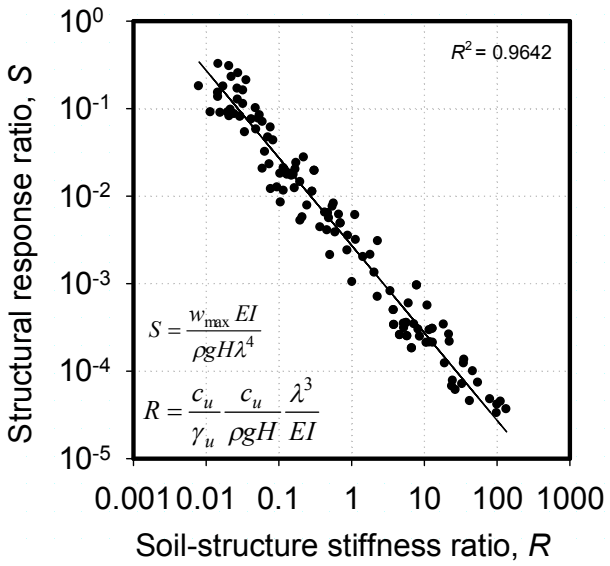

Figure 14 A new understanding of wall stiffness effects

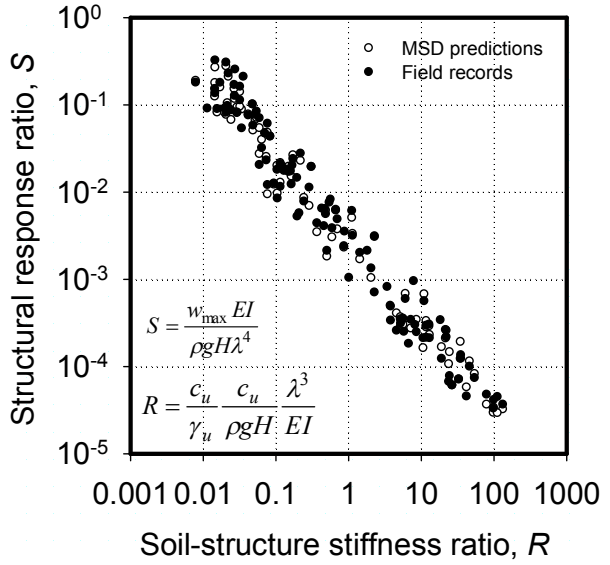

Figure 15 Comparing field data and MSD predictions

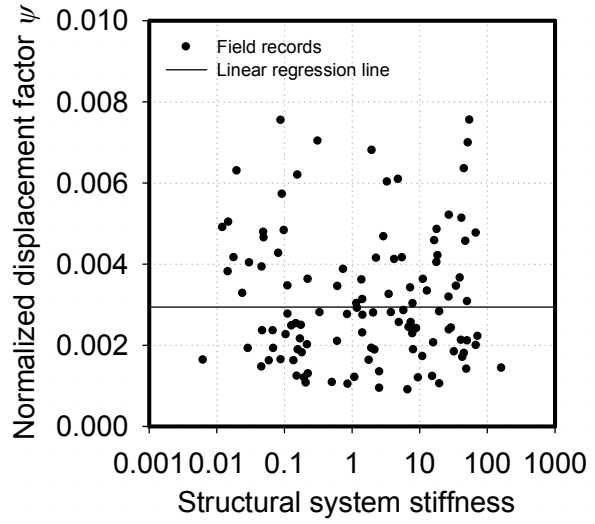

Figure 16 Field data plotted on ψ versus η

Equation 17 enables the engineer to estimate maximum wall displacement w_{max} using knowledge only of excavation depth H, clay depth D to a stiff stratum (to calculate λ from equation 10), soil density ρ and shear strength c_u at mid-depth $0.5D$, and the reference strain γ_u required for peak strength. But the possible variation by a factor of up to 2.9 must not be forgotten. This is emphasised in Figure 16 where the normalized displacement factor ψ is plotted on a linear scale against a non-dimensional structural system stiffness η where:

$$\eta = \frac{EI}{\rho_w g \lambda^4} \tag{18}$$

It is clear that structural stiffness does not bias the ground movements. Further work is under way to identify the sources of the remaining uncertainty.

4 DISCUSSION AND CONCLUSIONS

4.1 *Flowslides due to intense rainfall*

In the study by Take and Bolton (2004) the aim was to identify those circumstances in which steep slopes of loose silty sand might be most likely to exhibit violent flowsliding as a result of intense rainfall. The finding was that simple slope wetting would not produce flowsliding, at least in the tests that were conducted. However, a buried layer of permeable material, fed from above by percolating storm water, was able to reproduce the main features of flowslide events seen previously in Hong Kong. PIV revealed the triggering mechanism which also explained the basis of subsequent flowsliding. High pressure water attempting to escape from the buried reservoir provided temporary lubrication to the slipping soil mass.

This finding could be very helpful to agencies seeking to minimize public risk at minimum cost. A strategy could be to send engineers out into the field immediately after rainstorms and flag cases of slopes exhibiting seepage at their toes. Such slopes, and any other slopes for which a flowslide could have catastrophic consequences, could be perforated with horizontal drains at their toes.

Although the original quality of the evidence in favor of the triggering of Hong Kong fast flowslides by static liquefaction was weak, the GEO felt unable to reconsider the matter. In any event, by the time the centrifuge research had been conducted, over US$2B had already been spent on the re-engineering of slopes, and the frequency and severity of landslide occurrences had dropped very significantly.

4.2 *Ground movements around deep excavations*

Lam et al (2011) report centrifuge model tests of braced excavations constructed in flight. Deformation analysis by PIV revealed lifelike deformation mechanisms operative at small to moderate strains. These mechanisms in the field give rise to anxiety on behalf of the constructors of deep excavations, their neighbors, and also municipal authorities and government regulators.

It was contended that these mechanisms needed to be simplified in order to generate practical design rules. A new class of finite-strain deformation mechanism was therefore invoked, and used to make predictions of moderate ground movements through the Mobilizable Strength Design (MSD) method: Lam and Bolton (2011). This is the equivalent of an upper bound limit equilibrium analysis based on plastic work, but instead it uses the stress-strain data of the representative soil to predict ground movements from a global energy balance conducted for the mechanism in the working (service) state. The strain energy stored in the excavation support system can be included. When back-calculations were made of 110 deep excavations previously reported by respected authors, it was found that maximum wall movements were reproduced within a factor of 1.4 in over 90% of cases.

Furthermore, the quasi-closed-form nature of MSD calculations based on simplified deformation mechanisms and simplified parabolic stress-strain curves, led to the establishment of new dimensionless groups of parameters that control ground movements around excavations. It was shown, accordingly, that the stiffness of a retaining wall within the normal range (sheet piles, secant piles, diaphragm walls up to 1.2 m thick) makes a negligible contribution to limiting ground and wall movements. This finding may both prevent future failures in normally consolidated clays, and provide economies in overconsolidated clays where stiff diaphragm walls would be seen to be unnecessary, at least for the temporary works: Bolton et al (2010).

This work should contribute to the avoidance of collapse of deep retaining walls during the construction of deep excavations in soft clay. Such collapses happen quite frequently. Recent examples include the braced excavation for Sajinqiao subway station in Xi'an in August 2009, the braced excavation for the Xianghu subway station construction in Hangzhou in November 2008, the access tunnel to Suzhoujie Station under construction in Beijing in March 2007 and, most famously, the braced diaphragm wall excavation for approach tunnels to the Nicoll Highway subway station in Singapore in March 2004.

This last disaster is notable because the Government of Singapore held a Committee of Inquiry (COI) which reported in an open and accessible way on the background and the sequence of events. The consequences included the deaths of four construction workers, the closure of a main highway, the abandonment of the original subway excavation and its reconstruction on a fresh tunnel alignment. A view of the site immediately after the collapse, taken from the COI report (Magnus et al, 2005), is given in Figure 17.

Figure 17 Nicoll Highway subway construction collapse

Equation 17 demonstrated that wall bulging below the bottom prop of a deep excavation will have a magnitude proportional to the characteristic size λ of the mechanism, the shear strain γ_u required to mobilize the strength of the soil, and the square of the stability number of the excavation ($\rho gh/c_u$). Early evidence of wall movements as propped excavation proceeds can be back-analyzed to fix the value of the normalised displacement factor ψ which should thereafter remain roughly constant until the approach of total collapse.

On 17th April 2004, inclinometer 104 at the location of the collapse of 30th April, showed a deformation extending to $D \approx 40$ m below ground level, and with a bulge $w_{max} \approx 0.35$ m. Accepting an average wavelength $\lambda_{ave} \approx 20$ m, and the simplified MSD result $\gamma \approx 2w_{max}/\lambda_{ave}$ we find that the Singapore marine clay was already mobilizing 3.5% shear strain. But, according to the data of Figure 12, that takes it to failure. These elementary calculations could be carried out by any engineer with a pocket calculator.

The main aim of this paper has been to demonstrate that the systematic simplification of ground interaction mechanisms is as essential to achieving high practical impact in geotechnical engineering research as is the observation of such mechanisms in centrifuge tests. This should be the natural accompaniment to a forensic investigation of any geotechnical failure at full scale.

REFERENCES

Bolton, M.D. and Powrie, W. (1987) "The collapse of diaphragm walls retaining clay", Geotechnique 37 (3), 335-353.

Bolton, M.D. and Powrie, W. (1988) "Behaviour of diaphragm walls in clay prior to collapse", Geotechnique 38 (2), 167-189.

Bolton, M. D., Lam, S.Y. and Osman, A.S. (2008) "Supporting excavations in clay – from analysis to decision-making", 6th Int. Symp. Geotechnical Aspects of Underground Construction in Soft Ground, Shanghai, April, Vol.1, 12-25.

Bolton, M.D., Lam, S.Y. and Vardanega, P.J. (2010) "Predicting and controlling ground movements around deep excavations", Keynote Lecture in Geotechnical Challenges in Urban Regeneration, 11th Int. Conf. DFI-EFFC, London.

Haigh,S.K., Houghton,N.E., Lam, S.Y., Li,Z. and Wallbridge, P.W. (2010) "Development of a double-axis servo-actuator for novel centrifuge modeling", 7th Int. Conf. Physical Modelling in Geotechnics, Zurich, Vol.1, 239-244.

Jen, L.C. (1998). "The design and performance of deep excavations in clay". PhD thesis, Dept. of Civil and Environmental Engineering, MIT.

Knill, J. L., Lumb, P., Mackey, S., Mello, V. F. B., Morgenstern, N. R. and Richards, B. G., "Report of the Independent Review Panel on Fill Slopes", Government of Hong Kong, 1976.

Lam, S.Y. (2010) "Ground movements due to excavation in clay: physical and analytical models", PhD Thesis, Cambridge University.

Lam S.Y., Elshafie, M.Z.E.B., Haigh, S.K. and Bolton M.D (2011) "Development of a new apparatus for modeling deep excavations in a geotechnical centrifuge", International Journal of Physical Modeling in Geotechnics (accepted).

Lam, S.Y. and Bolton, M.D. (2011) "Energy conservation as a principle underlying mobilizable strength design for deep excavations", Journal Geotechnical and Geoenvironmental Engineering, ASCE, 132. (accepted)

Lee, Y.S. (2005) "Centrifugal modelling of landslide triggering mechanism in layered fill slopes", MPhil Thesis, Cambridge University.

Lee, Y.S., Cheuk, C.Y., and Bolton, M.D. (2008) "Instability caused by a seepage impediment in layered fill slopes", Canadian Geotechnical Journal, 45 (10), 1410-1425.

Magnus, R., Teh, C.I and Lau, J.M. (2005) "Report by the Committee of Inquiry into the incident at the MRT circle line worksite that led to the collapse of Nicoll Highway on 20th April 2004", Singapore Government.

O'Rourke, T.D. (1993) "Base stability and ground movement prediction for excavations in soft clay". Retaining Structures, Thomas Telford, London, 131-139.

Osman, A.S. and Bolton, M.D. (2006) "Ground movement predictions for braced excavations in undrained clay", J. Geotech. and Geo-env. Eng., ASCE, 132 (4), 465-477.

Take, W.A., Bolton, M.D., Wong, P.C.P. and Yeung, F.J. (2004) "Evaluation of landslide triggering mechanisms in model fill slopes", Landslides, Springer, 1 (3), 173-184.

White, D.J., Take, W.A. and Bolton, M.D. (2003). "Soil deformation measurement using Particle Image Velocimetry (PIV) and photogrammetry", Geotechnique, 53, (7), 619-632.

Wong, P.K.P (2003) "Centrifugal modelling of liquefaction failure of loose granitic fill slopes", MPhil Thesis, Cambridge University.

Yeung, F.J. (2002) "Modelling of the behaviour of saprolitic soil slopes under severe rainfall", MPhil Thesis, Cambridge University.